

1 **Modeling study of impacts on surface ozone of regional transport and**
2 **emission reductions over North China Plain in summer 2015**

3 Xiao Han^{1,2}, Lingyun Zhu³, Shulan Wang⁴, Xiaoyan Meng⁵, Meigen Zhang^{1,2}, Jun Hu⁴

4 ¹ *State Key Laboratory of Atmospheric Boundary Layer Physics and Atmospheric Chemistry, Institute of*
5 *Atmospheric Physics, Chinese Academy of Sciences, Beijing 100029, China.*

6 ² *College of Earth Science, University of Chinese Academy of Sciences, Beijing 100049, China*

7 ³ *Shanxi Province Institute of Meteorological Sciences, Taiyuan 030002, China*

8 ⁴ *Chinese Research Academy of Environmental Sciences, Beijing, 100012, China*

9 ⁵ *China National Environmental Monitoring Centre, Beijing, 100012, China*

10
11 Corresponding author:

12 Lingyun Zhu

13 Shanxi Province Institute of Meteorological Sciences

14 Xinjian Road 65#, Taiyuan, Shanxi province, China

15 Post code: 030002

16 Tel: 86-0351-4077738

17 Fax: 86-0351-4077738

18 E-mail: zhlyun@126.com

19 Meigen Zhang

20 E-mail: mgzhang@mail.iap.ac.cn

21
22 Other authors:

23 Xiao Han, E-mail: hanxiao@mail.iap.ac.cn

24 Shulan Wang, E-mail: shulanwang@foxmail.com

25 Xiaoyan Meng, E-mail: mengxy@cnemc.cn

26 Jun Hu, E-mail: hujun@craes.org.cn

Abstract

Tropospheric ozone (O_3) has replaced $PM_{2.5}$ or PM_{10} as the premier pollution in the North China Plain (NCP) during summer in recent years. A comprehensive understanding of the O_3 production in responding to the reduction of precursor emission over NCP is demanded urgently for the effective control policy design. In this study, the air quality modeling system RAMS-CMAQ (regional atmospheric modeling system-community multiscale air quality), coupled with the ISAM (integrated source apportionment method) module is applied to investigate the O_3 regional transport and source contribution features during a heavy O_3 pollution episode in June 2015 over NCP. The results show that the emission sources in Shandong and Hebei were the major contributors to O_3 production in the NCP. Not only the highest local contribution of O_3 mass burden, but also more than 30% contribution of O_3 mass burdens in Beijing and Tianjin were provided by the emission sources in these two provinces, respectively. On the other hand, the urban areas and most O_3 pollution regions of NCP were mainly dominated by the VOC-sensitive conditions, while "both control" and NO_x -sensitive conditions dominated the suburban and remote areas, respectively. Then, based on the sensitivity tests, the effects of several hypothetical scenarios of emission control on reducing the O_3 pollution were compared and discussed. The results indicated that the emission control of industry and residential sectors was the most efficient way if the emission reduction percentage was higher than 40%. However, when the emission reduction percentage dropped below 30%, the power plant sector could make significant contributions to the decrease in O_3 . The control strategies should be promptly adjusted based on the emission reduction, and the modeling system can provide valuable information for precisely choosing the emission sector combination to achieve better efficiency.

1. Introduction

In addition to the downward injection of stratospheric ozone (O_3), tropospheric O_3 is formed via a suite of photochemical reactions involving nitrogen oxides (NO_x), volatile organic compounds (VOCs), and sunlight. O_3 plays an important role in controlling the chemical composition and climate of the troposphere and harms vegetation and human health, especially in industrialized regions (Kleinman et al., 2002). In recent years, the emission of O_3 precursors, NO_x and VOCs, have increased substantially due to the economic growth, rapid population expansion, and urbanization in the North China Plain (NCP). During the summer, $PM_{2.5}$ or PM_{10} are replaced by O_3 as the premier pollution type in major urban areas (China Environmental Status Bulletin 2015).

Numerous studies have investigated the spatial and temporal distribution characteristics of O_3 in the NCP. Lin et al. (2008) analyzed the three-year observation data of the O_3 mixing ratio at a remote Global Atmosphere Watch site near Beijing and showed the seasonal variation features of the O_3 background value for the NCP. Tang et al. (2012) gathered two-year observation data of the O_3 mixing ratio for 22 sites (located in urban, rural, and coastal areas) during a field campaign in the NCP and coupled the data with the meteorological parameters from the WRF. The spatial and temporal variations of O_3 were through analyzed, and the O_3 - NO_x -VOCs sensitivity was initially investigated in this study. Ran et al. (2012) and Dufour et al. (2010) compared the O_3 seasonal variation features in megacities between the NCP and southern China. On the other hand, several studies have applied the chemistry transport model system to reproduce the three-dimensional O_3 continuous distribution characteristic and discussed the sensitivity of O_3 to precursor emissions (Wang et al., 2012; Nie et al., 2014).

Because of the strong emission of air pollutants, widespread haze clouds caused by serious air pollution have occurred frequently over the NCP (Tao et al., 2012; Wang et al., 2013; Li et al., 2016; Zhou et al., 2017). Aiming to solve this problem, the government has executed strict emission control strategies in recent years (Gao et al., 2016), which have yielded an initial effect. As reported by the China Environmental Status Bulletin, the mass loadings of sulfur dioxide (SO_2), NO_2 , $PM_{2.5}$, and PM_{10} steadily fell from 2013 to 2015. However, O_3 has become the only pollutant whose mass burden has continued to increase in the 74 experimental cities of China, and the mass concentration is expected to continue increasing (Deng et al., 2011). Therefore, there is an urgent need to prevent environmental and health hazards in the NCP resulting from the surface O_3 .

As a secondary pollutant, although the basic features of surface O_3 in the NCP are well known from

92 measurement or modeling studies, understanding the chemical links between O₃ and its two main precursors,
93 NO_x and VOC, is important for designing effective pollution reduction strategies (Castell et al., 2009). The
94 chemical transport model is an indispensable method for resolving the above issue, as it can quantify the
95 main physical and chemical mechanisms of pollutant formation and transport. Liu et al. (2010) used two
96 process analysis modules (integrated process rates and integrated reaction rates) embedded in CMAQ to
97 capture the dynamical and photochemical processes of O₃ formation in 2008 over China. As a result, the
98 influence and contribution of each important process can be distinguished and quantified. Tang et al. (2017)
99 also used the integrated process rates module for measurement data from a set of observation stations to
100 evaluate the sensitivity of O₃ production in June 2008 over the NCP. Xing et al. (2010) developed a
101 statistical response surface method which aimed at investigating ozone sensitivities to NO_x and VOC
102 emission changes and coupled it with CMAQ to analyze O₃ sensitivities to NO_x and VOCs emission
103 changes in 2005 over eastern China. The overall impacts from individual sources, including regional NO_x
104 and VOCs emission sources, have been evaluated using this modeling system. Li et al. (2008) applied a
105 tagged tracer method to the framework of NAQPMS to identify the transport contributions from various O₃
106 production regions to total O₃ levels in 2008 over central eastern China. This method can be used to
107 eliminate the errors caused by nonlinearities in the transport and fast photochemistry of O₃ and its
108 precursors.

109 In general, the substantial features of O₃ formation sensitivity and the contributions of regional-scale
110 transport have been discussed in these studies. However, more work needs to be done to achieve a
111 comprehensive understanding of O₃ behavior over the NCP, especially the source contribution approaches
112 of recent years. In this study, an air quality modeling system called RAMS-CMAQ (regional atmospheric
113 modeling system–community multiscale air quality) that is coupled with the ISAM (integrated source
114 apportionment method) module is applied to estimate the regional contributions of O₃ among major regions
115 of the NCP and to quantify the relative amount of O₃ originating from specific VOCs and NO_x emissions
116 sources. A unique method that can distinguish the O₃–NO_x–VOC sensitivity features is also used to identify
117 the precursor sensitivity regions and verify the results of the ISAM. In addition, the brute-force method is
118 applied to investigate the effect of reducing anthropogenic emissions on the O₃ mass burden. Therefore, the
119 precursor control type and contribution from specific geographic areas and emission sectors can be obtained,
120 and some valuable information can be provided for control strategies in the NCP.

121

2. Methodology

CMAQ (version 5.0.2), released in April 2014 by the US EPA ([https://www.airqualitymodeling.org/index.php?title=CMAQ_version_5.0.2_\(April_2014_release\)_Technical_Documentation&oldid=587](https://www.airqualitymodeling.org/index.php?title=CMAQ_version_5.0.2_(April_2014_release)_Technical_Documentation&oldid=587)), was applied over the NCP for 2-month simulations in January and June 2015. Several updates and revisions, such as the chemical process corresponding to NH₃ and SO₂ and the secondary aerosol formation of SOA (secondary organic aerosol) and nitrate, have been added in this version. The updated and expanded version of the carbon bond mechanism (CB05) (Sarwar et al., 2008) and the sixth-generation modal CMAQ aerosol model (AERO6) were applied to simulate the gas-phase chemistry mechanisms and formation and the dynamic processes of aerosols, respectively. The ISORROPIA model (version 1.7) was used to describe the thermodynamic equilibrium of gas-particle transformation (Nenes et al., 1999). The highly versatile RAMS numerical code (Cotton et al., 2003), which can well simulate the boundary layer and the underlying surface, is utilized to provide the meteorological fields for CMAQ. The mechanisms about secondary organic aerosol formation, on-line dust emission were modified for improving the simulation ability in China (Han et al., 2012; Li et al., 2017), and the information of underlying surface in China was also updated (Chen et al., 2018).

The anthropogenic emissions of major pollution species (NO_x, SO₂, VOCs, BC, OC, primary PM_{2.5}, and PM₁₀) were obtained from the monthly-based emission inventory, with 0.25°×0.25° horizontal resolution and four categories (industry, power, transport, and residential), which were developed to support the Model Intercomparison Study Asia (Li et al., 2015). The original version of this emission inventory was developed for Asia as a contribution to the TRACE-P (Transport and Chemical Evolution over the Pacific) Mission and ACE-Asia (Asian Pacific Regional Aerosol Characterization Experiment) (Streets et al., 2003). Additionally, the NO_x and NH₃ emissions from the soil and natural hydrocarbon emissions were obtained from the Global Emissions Inventory Activity 1°×1° global monthly inventory (Benkovitz et al., 1996). The Global Fire Emissions Database, Version 3 (FGEDv3.0; van der Werf et al., 2010), was applied to provide the biomass burning emissions from wildfires, savanna burning, and slash-and-burn agriculture. The VOCs and nitrogen oxides from flight exhaust, lighting, paint, fossil fuel, and other sectors were obtained from the regional emission inventory in Asia (REAS, Version 2, <http://www.jamstec.go.jp/frsgc/research/d4/emission.htm>) and the emission database for global atmospheric research (Olivier et al., 1994), respectively.

The ISAM module was used to track O₃ from different geographic regions and source types. This

152 source apportionment tool was developed from the TSSA (tagged species source apportionment; Wang et
153 al., 2009) in an early version of the CMAQ model. Compared with the previous version, the ISAM
154 improved the approach for the advection of tagged tracers and the tracking of precursor reactions and
155 increased the flexibility of the application by minimizing the amount of data preparation (Kwok et al., 2013).
156 An updated piecewise parabolic algorithm was applied to reasonably estimate the major dynamics
157 processes, including advection transport, vertical diffusion, and dry deposition. For the nonlinear gas-phase
158 chemical interactions, which are important for O₃ formation, a hybrid approach that employs the direct
159 sensitivity methods as linear equations using lower and upper triangular matrices, which is known as LU
160 decomposition (Yang et al., 1997), was applied for description. In addition, the ISAM uses two tracers for
161 individual nitrogen and VOC species to represent the O₃ chemical formation regime attributed to either
162 NO_x or VOC emission sources. As described by Kwok et al. (2014), the total concentration of O₃ in each
163 model grid cell is equal to the sum of O₃ tracers that were produced in either VOC- or NO_x-sensitive
164 conditions:

$$165 \quad O_3 \text{ bulk} = \sum_{tag} O_3 V_{tag} + \sum_{tag} O_3 N_{tag} \quad (1)$$

166 where O₃V_{tag} and O₃N_{tag} are the VOC-sensitive and NO_x-sensitive O₃ attributed to each tag source,
167 respectively. Therefore, the contribution from VOCs or NO_x can be tracked individually, and the precursor
168 control types in each grid can be deduced. Detailed information regarding the ISAM can be found in Kwok
169 et al. (2013).

170 The simulation has two layer grids. The coarse domain covers East Asia (Figure 1, D1), with a
171 horizontal grid spacing of 64 km and a total area of 6654 km×5440 km, and an inner domain (Figure 1, D2)
172 with a 16 km×16 km resolution is two-way nested with the outer one. The inner domain covers the major
173 regions of the NCP, including the megacity of Beijing, Tianjin, the capital city of the Shijiazhuang province,
174 Jinan, the industrial town of Tangshan, and the Hebei, Shandong, and Shanxi provinces. The simulation
175 used 15 vertical levels, of which nearly half were concentrated in the lowest 2 km, to improve the simulation
176 of the atmospheric boundary layer. Numerous previous studies have demonstrated that this modeling system
177 performs well in simulating the pollutant mass concentrations (Zhang et al., 2006; Han et al., 2014; Han et
178 al., 2016)

179

180 **3. Model evaluation**

181 The meteorological parameters, such as the temperature and wind field, are important impact factors

182 of ozone formation and transport. Therefore, the daily average temperature, relative humidity, wind speed,
183 and maximum wind direction in January and June 2015 were compared with the surface observation data
184 (released by the Chinese National Meteorological Center: <http://data.cma.cn/>) for Beijing, Tianjin,
185 Shijiazhuang, and Jinan. The comparison results are shown in Figure 2. The modeled temperature and
186 relative humidity are shown to generally coincide with the observations at all four of these stations, except
187 that some of the extreme high or low values appeared abruptly. The modeled wind speed, which could
188 reproduce the higher value in Tianjin and Jinan and lower value in Beijing and Shijiazhuang, also followed
189 the magnitude of observations well. However, a direct comparison between observed and modeled data is
190 difficult, especially for the wind direction. Besides the obviously impact of surrounding surface at each
191 measurement station, the time resolutions between observation (10 minute mean) and model output (1 hour)
192 were also different. Nevertheless, the north wind in winter and south wind in summer were generally
193 captured by the simulation results for all stations.

194 The modeled mass concentrations of O₃ and one of its precursors (NO₂) were compared with the hourly
195 observation data from the Ministry of Environmental Protection of China; the results are shown in Figures
196 3 and 4. The statistical parameters the means, standard deviation, and correlation coefficients between the
197 observations and simulations are listed in Tables 1 and 2. The nitrogen oxide and tropospheric ozone were
198 two kinds of typical trace gases with high chemical activity and relatively short lifetimes. The diurnal
199 change in Figures 3 and 4 is obvious, and the distinctive values of the mass concentrations between different
200 seasons can also be found. The simulation results also reproduced these important features, especially the
201 evident diurnal variation of O₃ at these four stations. The mass concentration of O₃ in summer was generally
202 higher than that in winter because of the strong photochemistry during the daytime in summer. On the other
203 hand, the metrics listed in Tables 1 and 2 were used to evaluate the model performance, following the study
204 of Yu et al. (2006). Most of the correlation coefficients were higher than 0.5 for NO₂ and 0.6 for O₃, which
205 indicates that the model performed well in reproducing the observation trend. The simulation results were
206 able to capture most of the pollution episodes during these two months. In addition, the standard deviations
207 between the observation and simulation of NO₂ and O₃ were also similar in most cases. Most of the mean
208 NO₂ concentration of simulation was generally similar with that of the observation in June, but about 25
209 $\mu\text{g m}^{-3}$ lower at Tianjin in January. As shown in Figure 3, the model missed some of the high values of
210 observation that appeared during the first half of January. The largest deviation of the modeled O₃, which
211 the mean mass burden was obviously higher than that of the observation and the correlation coefficient was

212 just 0.48, also appeared at Tianjin in January. Yu et al. (2010) reported similar results and noted that the
213 model might not well resolve the titration by NO in an urban area under a low O₃ mass burden background
214 by applying both the CB05 and SAPRC-99 mechanisms. Nevertheless, the comparison generally showed
215 that the model could basically reproduce the meteorological field and mass concentration and trends of O₃
216 and its precursor NO₂ during different seasons over the NCP.

218 4. Results and discussion

219 The surface spatial distributions of the monthly average values of the modeled NO_x, VOCs, and
220 maximum daily 8-hour average O₃ mass concentration (8H-O₃) for January and June 2015 are shown in
221 Figure 5. The monthly average wind field is also shown. The diffusion condition is shown to have been
222 weak due to the obviously smaller wind speed over Beijing, Tianjin, Hebei, Shandong, and northern Henan
223 in both January and June. In addition to the strong emission, the weak diffusion condition should be the
224 main reason for the high mass burden of NO_x and VOCs in these regions. In addition, the maximum values
225 were mainly concentrated in the urban areas of the NCP during these two months, including the following
226 five major pollution cities: Beijing, Tianjin, Shijiazhuang, Jinan, and Tangshan. However, the distribution
227 patterns between O₃ and the precursors were significantly different, which indicates that the formation and
228 transport processes of O₃ should be complex in the NCP. Unlike the seasonal variation of NO_x and VOCs,
229 the mass burden of O₃ in summer was obviously higher than that in winter because of the stronger
230 photochemical activity. The 8H-O₃ mass concentration, which exceeded the Grade II standard (160 μg m⁻³)
231 ³), was widespread throughout southern Beijing, Hebei and almost the entire areas of Tianjin and Shandong,
232 with values reaching 180-200 μg m⁻³ in the tri-province area of Hebei, Shandong, and Henan in June. The
233 serious O₃ pollution was mainly concentrated in the northwest part of the Shandong province.

234 The contribution of O₃ from the major NCP regions, including Beijing, Hebei, Shandong, Tianjin, and
235 Shanxi, was calculated using ISAM-CMAQ-RAMS; the results are shown in Figure 6 (NS: NO_x-sensitive
236 O₃) and Figure 7 (VS: VOC-sensitive O₃). The total percentage can be obtained by summing the
237 contributors of NS and VS and shown in Table 3. The distribution patterns of NS and VS contributions
238 were generally similar to each other. The mass contribution of O₃ in Shandong, Hebei, and Shanxi was
239 mainly provided by local anthropogenic sources, and the local contribution could reach 36.6%, 53.6%, and
240 45.0%. However, the local sources did not provide the primary contributions in Beijing (23.1%) and Tianjin
241 (14.9%), and the regional transport contributions from Hebei and Shandong could reach 35.2% and 37.3%

242 to these two cities, respectively. This feature clearly indicates that the regional transport of precursors
243 should be an important factor of O₃ pollution in Beijing and Tianjin. The contribution from Shanxi to other
244 regions was very small due to the hindrance to pollutant transport caused by the Taihang Mountains, which
245 are located to the east of the Shanxi province. The contribution from other regions to Shanxi was also very
246 low in corresponding as shown in Table 3. In addition, the contribution from Shandong provided at least
247 more than 65% to the mass burden of O₃ in the Bohai Sea. This feature explains the source of the large
248 value that appears over this area in Figure 4. On the other hand, the contribution of VS was obviously higher
249 than that of NS in Beijing, Tianjin, Hebei, and Shandong. Compared with the NS, the percentage of VS was
250 generally double in Beijing and Tianjin and more than 10% higher in all of Shandong and the southern part
251 of Hebei. In contrast, the contribution of NS was clearly higher than that of VS in Shanxi, which means
252 that the major role of the O₃ formation in Shanxi should be different from that in other regions.

253 To distinguish the O₃-NO_x-VOC sensitivity features, a method that is suitable for the results of three-
254 dimensional chemistry/transport models was applied to identify the precursor sensitivity regions in the NCP.
255 In addition to the base case, two sensitivity tests, which reduced 30% of the VOC emissions and 30% of
256 the NO_x emissions, respectively, within the entire model domain, were conducted. Then, the deviation of
257 the maximum daily 8H-O₃ between the base case and these two sensitivity tests could be utilized to
258 determine the precursor control types in each grid. Here, we used ΔO_{3V} and ΔO_{3N} to represent the variation
259 of the mass concentration of O₃ due to the reduction in VOC or NO_x emission, respectively (Sillman and
260 He, 2002; Sillman and West, 2009): (1) if the changes in ΔO_{3V} and ΔO_{3N} were both less than 4 $\mu\text{g m}^{-3}$, this
261 grid was likely controlled by neither NO_x nor VOCs; (2) if ΔO_{3N} increased to a value greater than 4 $\mu\text{g m}^{-3}$
262 and ΔO_{3V} decreased to a value less than 4 $\mu\text{g m}^{-3}$, this grid should be regarded as “NO_x titration”; (3) if
263 ΔO_{3V} decreased by more than 4 $\mu\text{g m}^{-3}$, with this reduction being twice as large as the ΔO_{3N} reduction (or
264 ΔO_{3N} increase), this grid was likely controlled by VOCs; (4) if ΔO_{3N} decreased by more than 4 $\mu\text{g m}^{-3}$, with
265 the reduction being twice as large as the ΔO_{3V} reduction, this grid was likely controlled by NO_x; (5) if ΔO_{3N}
266 and ΔO_{3V} both decreased by more than 4 $\mu\text{g m}^{-3}$ and the ratio between them was less than 2:1 or 1:2, this
267 grid was likely controlled by both NO_x and VOCs. Details regarding the identification explained above can
268 be found in Figure 8(f). The frequency of precursor control types in each grid in June was determined and
269 is shown in Figure 8(a-e). The NO_x titration scarcely appeared in the model domain. The frequency of the
270 “no control” type entirely exceeded 50% over the background regions when the O₃ mass burden was lower
271 than 120 $\mu\text{g m}^{-3}$ and gradually decreased as the O₃ mass burden increased. Over the O₃ pollution areas, a

272 grid with a “no control”-type frequency higher than 10% was seldom found. Specific to the considered
273 regions, the urban area of Beijing, Tianjin, Tangshan, southern Hebei, and northern and western Shandong
274 were mainly under VOC control, while the outer suburb of Beijing, all of Shanxi, and northern Hebei were
275 mainly under NO_x control. The “both control” type generally appeared in the transitional zone between
276 NO_x and VOC control. Compared with the results shown in Figures 6 and 7, the distribution feature of NO_x
277 and VOC contributions highly coincided with that of the O₃ precursor sensitivity types, which demonstrated
278 that this method is reliable.

279 In addition to the contribution feature of emission sources estimated using the ISAM, the effect of
280 reducing anthropogenic emissions on the O₃ mass burden was also necessary to learn because the formation
281 of O₃ from NO_x and VOC emissions is a typical nonlinear process. The brute-force method, which can
282 realistically capture the nonlinear processes of secondary pollutant formation, was applied. Therefore,
283 several sensitivity tests were designed, as shown in Table 4. First, the zero-out (100% source removal)
284 simulations of four major sectors, i.e., industry, power plants, transport, and residential (sensitivity tests ZI,
285 ZP, ZT, and ZR, respectively), were conducted to evaluate the efficiency of emission reduction for different
286 sources in the NCP. Figure 9 presents the results of the brute-force sensitivity tests and the NO_x and VOC
287 emission flux of each major sector. The removal of the industry sector is shown to have been the most
288 efficient way to decrease the O₃ mass burden, and the variation of 8H-O₃ between 20 and 30 μg m⁻³ was
289 generally concentrated in the high mass concentration regions. The main reason is likely that the VOC
290 emission flux of the industry sector was significantly higher than that of the other sectors. Removal of the
291 residential sector could also decrease the O₃ mass burden in most of the VOC control regions due to its
292 VOC emission flux being notably higher than that of NO_x. In contrast, removal of the transport and power
293 plant sectors could not effectively reduce the O₃ mass burden and even increased the mass burden in high
294 pollution areas, such as southern Beijing, Tianjin, Tangshan, southern Hebei, Jinan, and other parts of
295 Shandong. The NO_x emission flux of these two kinds of sectors was clearly higher than that of VOCs,
296 especially for the power plant sector. It also caused the 8H-O₃ mass burden to decrease by 5-10 μg m⁻³ in
297 Shanxi as a result of the removal of the power plant sector. It can be deduced that the ambient NO_x mass
298 burden should be plentiful and restrained the O₃ formation because of the reaction below:



300 Therefore, the environmental condition would be benefit for the O₃ formation when the NO_x mass burden
301 decrease due to power plant or transport sector removal. In summary, if we focus on the major pollution

302 regions of the NCP, including Beijing, Tianjin, Hebei, and Shandong, reduction of the industry and
303 residential emission sectors should be an effective way to control the O₃ mass burden during heavy O₃
304 pollution episodes.

305 In addition, the realistic pollution control strategies are supposed to be applied to a specific sector in
306 the high emission regions (HERs) and used to develop a comprehensive reduction scheme; thus, a detailed
307 analysis is necessary to investigate more accurate and practical strategies. Other than applying the simple
308 zero-out sensitivity test over entire objective regions, we selected the regions that include cities and towns
309 with high anthropogenic emission flux in the Beijing, Tianjin, Hebei, and Shandong (BTHS) region to more
310 accurately match real emission control. Figure 10 presents the selected regions and the emission flux of
311 NO_x and VOCs from the industry sector, residential sector, and multiple combinations. First, the change in
312 8H-O₃ mass concentration associated with the anthropogenic emission in selected regions (Figures 10(i)
313 and 10(j)) was compared with that in the entire BTHS region (sensitivity tests A20%-HERs and A20%-
314 BHTS), as shown in Figures 11(a) and 11(b), respectively. The distribution patterns of the 8H-O₃ mass
315 burden variation were notably similar to each other, and the positive and negative values generally appeared
316 in the same regions. However, the negative value in Figure 11(b) was clearly higher than that in Figure
317 11(a). This disparity indicates that significant overestimation of the O₃ mass burden variation might occur
318 when we conduct a brute-force sensitivity test with broad reductions in emissions in the entire objective
319 regions.

320 According to the results of the zero-out sensitivity tests, the industry and residential sectors were the
321 major emission sources of O₃, while the power plant sector did not benefit O₃ formation. Thus, the effects
322 of reducing these industry and residential sectors were estimated using the brute-force method with 20%
323 emission intensity in the selected regions of BTHS (Figures 10(a) and 10(b)). Figures 11(c) and 11(d) show
324 the variation of O₃ associated with the industry and residential emission sectors (sensitivity tests I20%-
325 HER and R20%-HER), respectively. The 8H-O₃ mass concentration could decrease by 10-12 μg m⁻³ in
326 most of Shandong, especially in the strong polluted regions shown in Figure 11(c). In contrast, the value
327 slightly increased in the urban areas of Shijiazhuang, Tianjin, and Tangshan. In Figure 5(f), the 8H-O₃ mass
328 burden was relatively lower in these regions. Thus, the O₃ mass burden can be decreased rapidly by
329 controlling the industry emissions under a heavy O₃ pollution background. Figure 11(d) shows that the 8H-
330 O₃ mass concentration decreased overall in BTHS, though the range was only 1-5 μg m⁻³. The likely main
331 reason is that the emission of VOCs was higher than that of NO_x from the residential sector, while the

332 emission intensity from the residential sector was relatively lower than that from industry. The mass burden
333 of O₃ can also be reduced by controlling the residential emissions in the urban areas of Shijiazhuang, Tianjin,
334 and Tangshan.

335 In addition, the influence of different combinations of emission sectors in BTHS was discussed.
336 Figures 11(e) and 11(f) present the change in 8H-O₃ mass concentration associated with a 20% emission
337 intensity for both the industry and residential sectors (sensitivity test IR20%-HERs) and the industry,
338 transport, and residential sectors (sensitivity test ITR20%-HERs), respectively. The O₃ mass burden
339 generally decreased sharply in BTHS, as shown in Figure 11(e), especially in the regions of Shandong with
340 heavy pollution. The range and magnitude of decrease can obviously be enhanced while considering the
341 reduction of the transport sector, as shown in Figure 11(f). Notably, the mass concentration of 8H-O₃ could
342 decrease from 180-200 μg m⁻³ to 160-180 μg m⁻³ in the polluted regions of BTHS. Compared with the zero-
343 out sensitivity test in Figure 9, the decrease in 8H-O₃ mass burden in Figure 11(f) was still clearly lower
344 than that of ZI. This deviation indicates that the contribution source from other regions except BTHS should
345 also be important. Even though 80% of the emission intensity was removed, the reduction in 8H-O₃ mass
346 concentration still barely exceeded 20 μg m⁻³ in the NCP, as shown in Figures 11(c), 11(d), and 11(e), which
347 means that it was difficult to keep the O₃ mass burden under the Grade II standard by controlling only the
348 industry and residential emission sectors in HERs.

349 Therefore, more brute-force sensitivity tests with HERs emissions varied from 50% to 0% were
350 conducted. The regional average 8H-O₃ mass concentrations in Beijing, Tianjin, Shijiazhuang, Jinan, and
351 Tangshan with changes in emission are shown in Figure 12. Three series of sensitivity tests were conducted:
352 reduction of the IR (industry and residential), ITR (industry, transport, and residential) and All (industry,
353 transport, power plant, and residential) emission sectors. As shown, the 8H-O₃ mass concentration was
354 higher than 160 μg m⁻³ in all five cities, while the emission percentage was 100%. When the emissions
355 reduced to 50%, the 8H-O₃ mass concentrations of these three series slightly decreased for Beijing, Tianjin,
356 Tangshan, and Jinan but increased for Shijiazhuang. The decrease in 8H-O₃ mass concentration as a result
357 of reducing the IR emission was similar to that of the ITR emission when the emissions were reduced from
358 50% to 40% for all five cities but was not significant when the reduction was less than 40%. The lines
359 corresponding to the ITR and All emission sectors generally decreased coherently for these five cities when
360 the emissions were reduced from 50% to 30%. However, the effect of the ITR reduction was obviously
361 weaker than that of the All reduction when the reduction was less than 30%. The decrease in 8H-O₃ mass

burden exceeded $12 \mu\text{g m}^{-3}$ when the All emission reduction was least, and the air quality in all five of these cities could reach the Grade II standard. This phenomenon indicated that the influence of the transport and power plant emission sectors on the decrease in O_3 mainly occurred after removing 60% of the IR or 70% of the ITR emission intensity, respectively. Thus, an emission control sequence for different sectors should be considered when exploring more effective strategies.

5. Conclusions

In this study, an air quality modeling system referred to as RAMS-CMAQ was applied to simulate the O_3 mass concentration, and several sensitivity tests were conducted to investigate the O_3 pollution and to discuss the relationship between O_3 production and emission contributions over the NCP in January and June of 2015. First, the modeled daily meteorological factors (temperature, relative humidity, and wind field) and hourly mass concentrations of O_3 and its precursor NO_2 were compared with ground-based observation data to evaluate the accuracy and reliability. The simulation results were generally good and able to broadly capture the values and variation trend of the observation data. Focusing on the heavy O_3 pollution period in June, an advanced source apportionment tool called ISAM was coupled with RAMS-CMAQ and applied to estimate the regional transport contributions, with individual tracers for nitrogen and VOC species used to represent the O_3 chemical formation regime attributed to either NO_x or VOC emission sources in the NCP. Then, a unique method that is suitable for three-dimensional chemistry/transport models was used to distinguish the O_3 - NO_x -VOC sensitivity features and identify the precursor sensitivity in each grid of the model domain. Therefore, the O_3 mass burden sensitivities to NO_x and VOC emission changes and the correlative regional transport contribution features among major anthropogenic source regions in the NCP can be clearly investigated using these methods. In addition, several brute-force sensitivity tests were conducted to discuss the role of the main anthropogenic emission sectors on reducing the O_3 mass burden, and an attempt was made to provide valuable suggestions for exploring more effective strategies for preventing O_3 pollution. The results are summarized as follows:

1. The simulation results show that the seasonal variation of O_3 was significant and that the heavy mass burden of 8H- O_3 , which exceeded the Grade II standard, generally occurred in southern Beijing, Hebei and almost all of Tianjin and Shandong in June. The mass burden of 8H- O_3 reached $180\text{-}200 \mu\text{g m}^{-3}$ mainly in the tri-province area of Hebei, Shandong, and Henan. The distribution pattern and seasonal variation of 8H- O_3 were obviously different from those of its precursors, which indicates that the formation and

392 transport processes of O₃ should be complex in the NCP.

393 2. The results of RAMS-CMAQ-ISAM show that the emission sources in Shandong and Hebei were
394 the major contributors to O₃ production in the NCP. In addition to these two provinces, the O₃ mass burden
395 in Beijing and Tianjin was also significant. The emissions from Hebei and Shandong contributed 15-20%
396 and 5-10% to Beijing and 10-20% and 15-20% to Tianjin, respectively. However, the O₃ mass burden in
397 these two provinces was generally contributed by the provinces themselves. The results also show that the
398 contribution of VS was clearly higher than that of NS in Beijing, Tianjin, Hebei, and Shandong, which
399 indicates that the O₃ mainly originated from VOC emission sources. On the other hand, the emission sources
400 in the Shanxi province almost had no impact on the O₃ mass burden in other regions of the NCP due to the
401 hinderance to pollutant transport provided by the Taihang Mountains.

402 3. The results of identification of the O₃-NO_x-VOC sensitivity feature show that the VOC control
403 mainly occurred over all of Tianjin and Tangshan and southern Beijing (urban area) and Hebei, where the
404 O₃ mass concentration reached 160-180 μg m⁻³. The north central part of Shandong and urban area of Jinan
405 were also mainly under the VOC control. The frequencies of VOC control and the "both control" type was
406 generally equal in the region of Hebei and Shandong where the O₃ mass concentration reached 180-200 μg
407 m⁻³. The NO_x control generally appeared in the regions of the NCP where the O₃ mass concentration reached
408 120-160 μg m⁻³. In the major cities with O₃ pollution, including Beijing, Tianjin, Shijiazhuang, and Jinan,
409 the O₃-NO_x-VOC sensitivity feature was the same: VOC control dominated the urban area, while "both
410 control" and NO_x control dominated the suburban and remote areas, respectively.

411 4. The results of the zero-out sensitivity tests show that the IR emission sectors were two important
412 contributors to ozone formation, as they were the major sources of VOCs, while the power plant emission
413 sector did not benefit O₃ pollution control in the high mass burden regions due to the greater emission of
414 NO_x versus VOCs.

415 On the other hand, the results of the brute-force sensitivity tests show that the effects of IR, ITR, and
416 All emission control on the decrease in O₃ were similar when their reduction percentages were higher than
417 40%. Meanwhile, the effects of ITR and All emission control were similar while the reduction percentages
418 were higher than 30%. When the reduction percentage dropped below 30%, the nonlinearity of O₃
419 formation was notable, and the power plant sector could make significant contributions to the decrease in
420 O₃. Thus, the control strategies should be promptly adjusted based on the emission reduction, and the
421 emission sector combination should be precisely chosen to achieve better efficiency. The modeling system

422 allows us to capture valuable information regarding how to choose the correct sequence and efficient
423 combinations by exploring the key thresholds from the bulk of sensitivity tests regarding crucial parameters.

424

425 **Acknowledgments**

426 This study was supported by the Strategic Priority Research Program of the Chinese Academy of Sciences
427 (XDA19040204) and the National Key R&D Program of China (2017YFB0503901), and the National
428 Natural Science Foundation of China (41475098).

429

430

431

432

433

434

435

436

437

438

439

440

441

442

443

444

445

446

447

448

449

450

451

References

- Benkovitz, C. M., Schultz, M.T., Pacyna, J., Tarrason, L., Dignon, J., Voldner, E.C., Spiro, P.A., Logan, A., and Graedel, T.E.: Global gridded inventories of anthropogenic emissions of sulfur and nitrogen, *J. Geophys. Res.*, 101(29), 239-253, 1996.
- Castell, N., Stein, A., Mantilla, E., Salvador, R., and Millan, M.: Evaluation of the use of photochemical indicators to assess ozone-NO_x-VOC sensitivity in the Southwestern Iberian Peninsula, *J. Atmos. Chem.*, 63(1), 73-91, 2009.
- Chen, L., Zhang, M., Zhu, J., Wang, Y., Skorokhod, A.: Modeling Impacts of Urbanization and Urban Heat Island Mitigation on Boundary Layer Meteorology and Air Quality in Beijing Under Different Weather Conditions, *J. Geophys. Res.*, 123(8), 4323-4344, 2018.
- Cotton, W. R., Pielke, R. A., Walko, R. L., Liston, G. E., Tremback, C. J., Jiang, H., McAnelly, R. L., Harrington, J. Y., Nicholls, M. E., Carrjo, G. G., and McFadden, J. P.: RAMS 2001: current status and futures directions, *Meteor. Atmos. Phys.*, 82, doi:10.1007/s00703-001-0584-9, 2003.
- Deng, X., Zhou, X., Wu, D., Tie, X., Tan, H., Li, F., Bi, X., Deng, T., and Jiang, D.: Effect of atmospheric aerosol on surface ozone variation over the Pearl River Delta region, *Sci. China Earth Sci.*, 54(5), 744-752, 2011.
- Dufour, G., Fremenko, M., Orphai, J., and Flaud, J.: IASI observations of seasonal and day-to-day variations of tropospheric ozone over three highly populated areas of China: Beijing, Shanghai, and Hong Kong, *Atmos. Chem. Phys.*, 10, 3787-3801, 2010.
- Gao, W., Tang, G., Ji, D., and Wang, Y.: Implementation effects and countermeasures of China's air pollution prevention and control action plan, *Res. Environ. Sci.*, 29(11), 1567-1574, 2016. (In Chinese)
- Han, X., Ge, C., Tao, J., Zhang, M., Zhang, R.: Air Quality Modeling for a Strong Dust Event in East Asia in March 2010, *Aerosol Air Qual. Res.*, 12: 615-628.
- Han, X., Zhang, M., Gao, J., Wang, S., Chai, F.: Modeling analysis of the seasonal characteristics of haze formation in Beijing, *Atmos. Chem. Phys.*, 14, 10231-10248, 2014.
- Han, X., Zhang, M., Zhu, L., Skorokhod, A.: Assessment of the impact of emissions reductions on air quality over North China Plain, 7, 249-259, 2016.
- Kleinman, L. I., Daum, P. H., Lee, Y. N., Nunnermacker, L. J., Springston, S. R., Lloyd, J., and Rudolph, J.: Ozone production efficiency in an urban area, *J. Geophys. Res.*, 107, D23, 23, 2002.
- Kwok, R. H. F., Baker, K. R., Napelenok, S. L., and Tonnesen, G. S.: Photochemical grid model implementation and application of VOC, NO_x, and O₃ source apportionment, *Geosci. Model Dev.*, 7(5), 99-114, 2014.
- Kwok, R., Napelenok, S., and Baker, K.: Implementation and evaluation of PM_{2.5} source contribution analysis in a photochemical model, *Atmos. Environ.*, 80, 398-407, 2013.
- Li, H., Zhang, Q., Chen, C., Wang, L., Wei, Z., Zhou, S., Parworth, C., Zheng, B., Canonaco, F., Prevot, A., Chen, P., Zhang, H., and He, K.: Wintertime aerosol chemistry and haze evolution in an extremely polluted city of North China Plain: significant contribution from coal and biomass combustions, *Atmos. Chem. Phys.*, 17, 4751-4768, 2017.
- Li, J., Zhang, M., Wu, F., Sun, Y., Tang, G.: Assessment of the impacts of aromatic VOC emissions and yields of SOA on SOA concentrations with the air quality model RAMS-CMAQ, *Atmos. Environ.*, 158, 105-115.
- Li, M., Zhang, Q., Kurokawa, J., Woo, H., He, K., Lu, Z., Ohara, T., Song, Y., Streets, D., Carmichael, G., Cheng, Y., Huo, H., Liu, F., Su, H., and Zhang, B.: MIX: a mosaic Asian anthropogenic emission

496 inventory for the MICS-Asia and the HTAP projects, *Atmos. Chem. Phys. Discuss*, 15, 34813-34869,
497 2015.

498 Lin, W., Xu, X., Zhang, X., and Tang, J.: Contributions of pollutants from North China Plain to surface
499 ozone at the Shangdianzi GAW Station, *Atmos. Chem. Phys.*, 8, 5889-5898, 2008.

500 Liu, X., Zhang, Y., Xing, J., Zhang, Q., Wang, K., Streets, D., Jang, C., Wang, W., and Hao, J.:
501 Understanding of regional air pollution over China using CMAQ, part II. Process analysis and
502 sensitivity of ozone and particulate matter to precursor emissions, *Atmos. Environ.*, 44, 3719-3727,
503 2010.

504 Nenes, A., Pilinis, C., and Pandis, S.N.: Continued development and testing of a new thermodynamic
505 aerosol module for urban and regional air quality models, *Atmos. Environ.*, 33, 1553-1560, 1999.

506 Nie, T., Li, X., Wang, X., Shao, M., and Zhang, Y.: Characteristics of the Spatial Distributions of Ozone-
507 Precursor Sensitivity Regimes in Summer over Beijing, *Acta Scientiarum Naturalium Universitatis*
508 *Pekinensis*, 50(3), 557-564, 2014. (in Chinese)

509 Olivier, J., Bouwman, A., Maas, C., and Berdowski, J.: Emission database for global atmospheric research,
510 *Environ. Monit. Assess.*, 31, 93-106., 1994.

511 Ran, L., Zhao, C., Xu, W., Han, M., Lu, X., Han, S., Lin, W., Xu, X., Gao, W., Yu, Q., Geng, F., Ma, N.,
512 Deng, Z., and Chen, J.: Ozone production in summer in the megacities of Tianjin and Shanghai,
513 China: a comparative study, *Atmos. Chem. Phys.*, 12, 7531-7542, 2012.

514 Sarwar, G., Luecken, D., Yarwood, G., Whitten, G. Z., Carter, W. P. L.: Impact of an updated carbon bond
515 mechanism on predictions from the CMAQ modeling system: preliminary assessment, *J. Appl.*
516 *Meteor. Climatol.*, 47, 3-14, 2008.

517 Sillman, S. and He, D.: Some theoretical results concerning O₃-NO_x-VOC chemistry and NO_x-VOC
518 indicators, *J. Geophys. Res.*, 107(D22): ACH-1-ACH 26-15, 2002.

519 Sillman, S. and West, J.: Reactive nitrogen in Mexico City and its relation to ozone-precursor sensitivity:
520 results from photochemical models, *Atmos. Chem. Phys.*, 9, 3477-3489, 2009.

521 Streets, D., Bond, T., Carmichael, G., Fernandes, S., Fu, Q., He, D., Klimont, Z., Nelson, S. M., Tsai, N. Y.,
522 Wang, : An inventory of gaseous and primary aerosol emissions in Asia in the year 2000, *J. Geophys.*
523 *Res.*, 108, DOI: 10.1029/2002JD003093, 2003.

524 Tang, G., Wang, Y., Li, X., Ji, D., Hsu, S., Gao, X.: Spatial-temporal variations in surface ozone in Northern
525 China as observed during 2009–2010 and possible implications for future air quality control
526 strategies, *Atmos. Chem. Phys.*, 12, 2757-2776, 2012.

527 Tang, G., Zhu, X., Xin, J., Hu, B., Tao, S., Sun, Y., Zhang, J., Wang, L., Cheng, M., Chao, N., Kong, L., Li,
528 X., and Wang, Y.: Modelling study of boundary-layer ozone over northern China - Part I: Ozone
529 budget in summer, *Atmos. Res.*, 187, 128-137, 2017.

530 Tao, M., Chen, L., Su, L., and Tao, J.: Satellite observation of regional haze pollution over the North China
531 Plain, *J. Geophys. Res.*, 117, D12203, doi:10.1029/2012JD017915, 2012.

532 van der Werf, G. R., Randerson, J. T., Giglio, L., Collatz, G. J., Mu, M., Kasibhatla, P. S., Morton, D. C.,
533 DeFries, R. S., Jin, Y., van Leeuwen, T. T.: Global fire emissions and the contribution of deforestation,
534 savanna, forest, agricultural, and peat fires (1997-2009), *Atmos. Chem. Phys.*, 10, 11707-11735, 2010.

535 Wang, X., Sun, M., Yang, T., and Wang, Z.: Interdecadal change in frequency of dust-haze episodes in
536 North China Plain, *Clim. Environ. Res.*, 18, 165–170, 2013 (in Chinese).

537 Wang, Y., Konopka, P., Liu, Y., Chen, H., Muller, R., Ploger, F., Riese, M., Cai, Z., and Lu, D.: Tropospheric
538 ozone trend over Beijing from 2002–2010: ozonesonde measurements and modeling analysis, *Atmos.*
539 *Chem. Phys.*, 12, 8389-8399, 2010.

- 540 Wang, Z. S., Chien, C. J., Tonnesen, G. S.: Development of a tagged species source apportionment
541 algorithm to characterize three-dimensional transport and transformation of precursors and secondary
542 pollutants, *J. Geophys. Res.*, 114, D21. DOI: 10.1029/2008JD010846, 2009.
- 543 Wu, R. and Xie, S.: Spatial Distribution of Ozone Formation in China Derived from Emissions of Speciated
544 Volatile Organic Compounds, *Environ. Sci. Technol.*, 51(5), 2574-2583, 2017.
- 545 Xing, J., Wang, S., Zhu, Y.: Nonlinear response of ozone to precursor emission Changes in China: A
546 modeling study using response surface methodology, *Atmos. Chem. Phys.*, 11(10):5027-5044, 2010.
- 547 Yang, Y., Wilkinson, J., and Russell, A.: Fast, direct sensitivity analysis of multi-dimensional
548 photochemical models, *Environ. Sci. Technol.*, 31(10), 2859–2868, 1997.
- 549 Yu, S. C., Eder, B., Dennis, R., Chu, S. H., and Schwartz, S.: New unbiased symmetric metrics for
550 evaluation of air quality models, *Atmos. Sci. Lett.*, 7, 26–34, 2006.
- 551 Yu, S., Mathur, R., Sarwar, G., Kang, D., Tong, D., Pouliot, G. and Pleim, J.: Eta-CMAQ air quality
552 forecasts for O₃ and related species using three different photochemical mechanisms (CB4, CB05,
553 SAPRC-99): comparisons with measurements during the 2004 ICARTT study, *Atmos. Chem. Phys.*,
554 10, 3001–3025, 2010.
- 555 Zhang, M., Uno, I., Zhang, R., Han, Z., Wang, Z., and Pu, Y.: Evaluation of the Models-3 Community
556 Multi-scale Air Quality (CMAQ) modeling system with observations obtained during the TRACE-P
557 experiment: comparison of ozone and its related species, *Atmos. Environ.*, 40, 4874-4882, 2006.
- 558 Zhou, S., Yang, L., Gao, R., Wang, X., Gao, X., Nie, W., Xu, P., Zhang, Q., and Wang, W.: A comparison
559 study of carbonaceous aerosols in a typical North China Plain urban atmosphere: Seasonal variability,
560 sources and implications to haze formation, *Atmos. Environ.*, 149, 95-103, 2017.

561
562
563
564
565
566
567
568
569
570
571
572
573
574
575
576
577
578
579
580
581
582
583

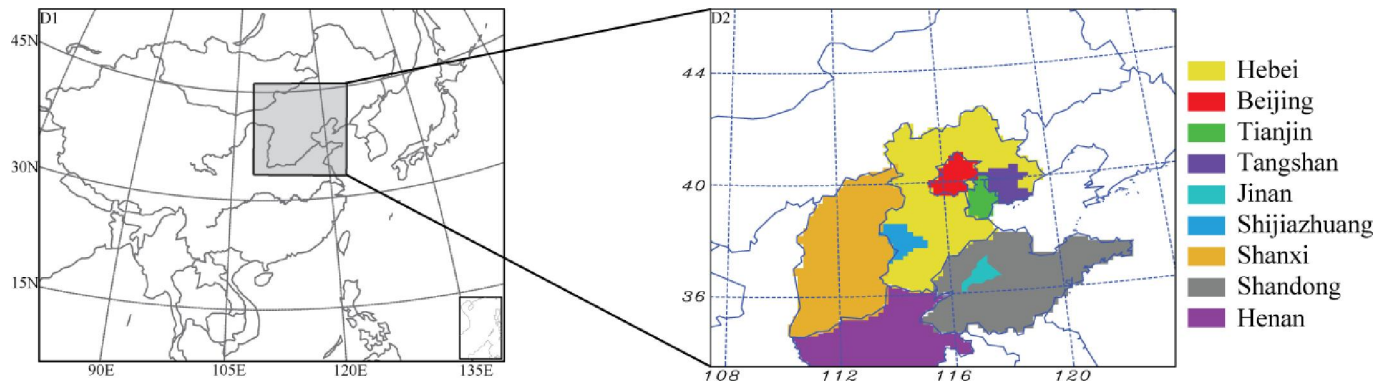
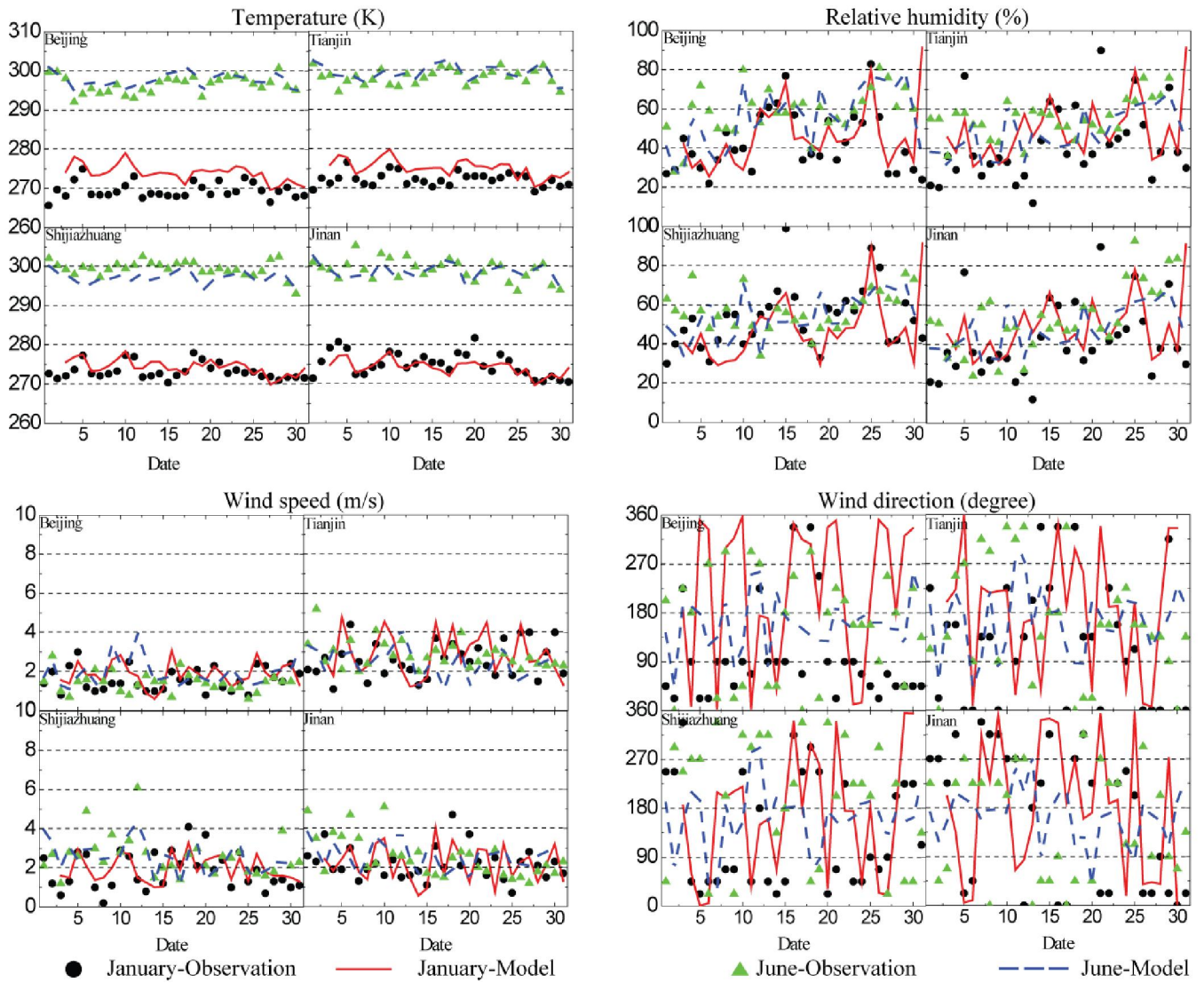
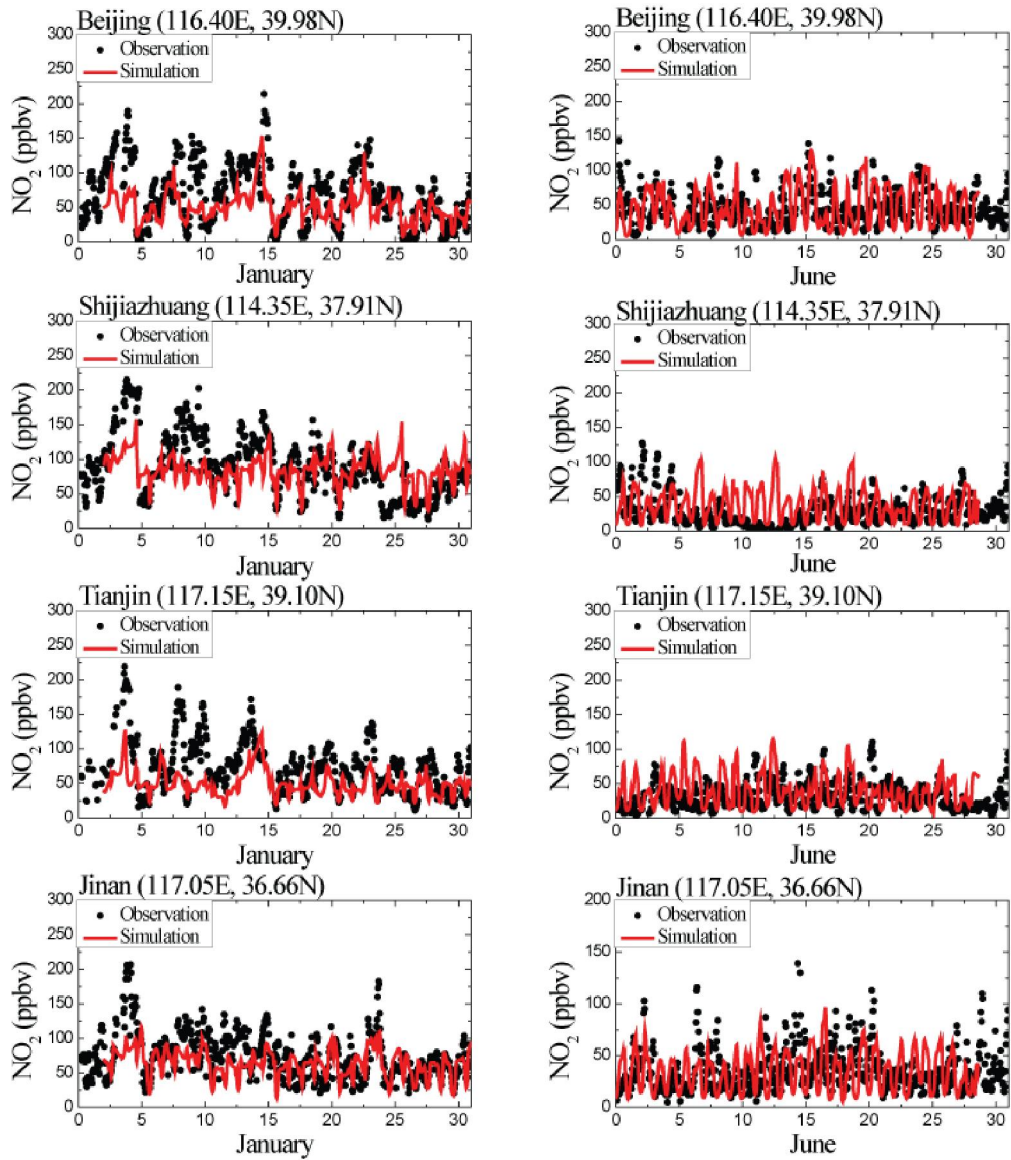


Figure 1 The model domain of this study, and the geographic locations of Beijing, Tianjin, Tangshan, Hebei, Shijiazhuang, Shanxi, Shandong, Jinan, and Henan.

584
 585
 586
 587
 588
 589
 590
 591
 592
 593
 594
 595
 596
 597
 598
 599
 600
 601
 602
 603
 604
 605
 606
 607
 608
 609
 610
 611
 612
 613
 614
 615
 616
 617
 618
 619



620
 621 Figure 2. Observed and modeled daily average temperatures (K), relative humidity (%), wind speed (m/s), and maximum
 622 wind direction at four stations in January and June 2015.
 623
 624
 625
 626
 627
 628
 629
 630
 631
 632
 633
 634
 635
 636



637
 638 Figure 3. Observed (black circles) and modeled (red solid lines) hourly mass concentrations ($\mu\text{g m}^{-3}$) of NO₂ at Beijing,
 639 Shijiazhuang, Tianjin, and Jinan in January and June 2015.
 640
 641
 642
 643
 644
 645
 646
 647
 648
 649
 650
 651

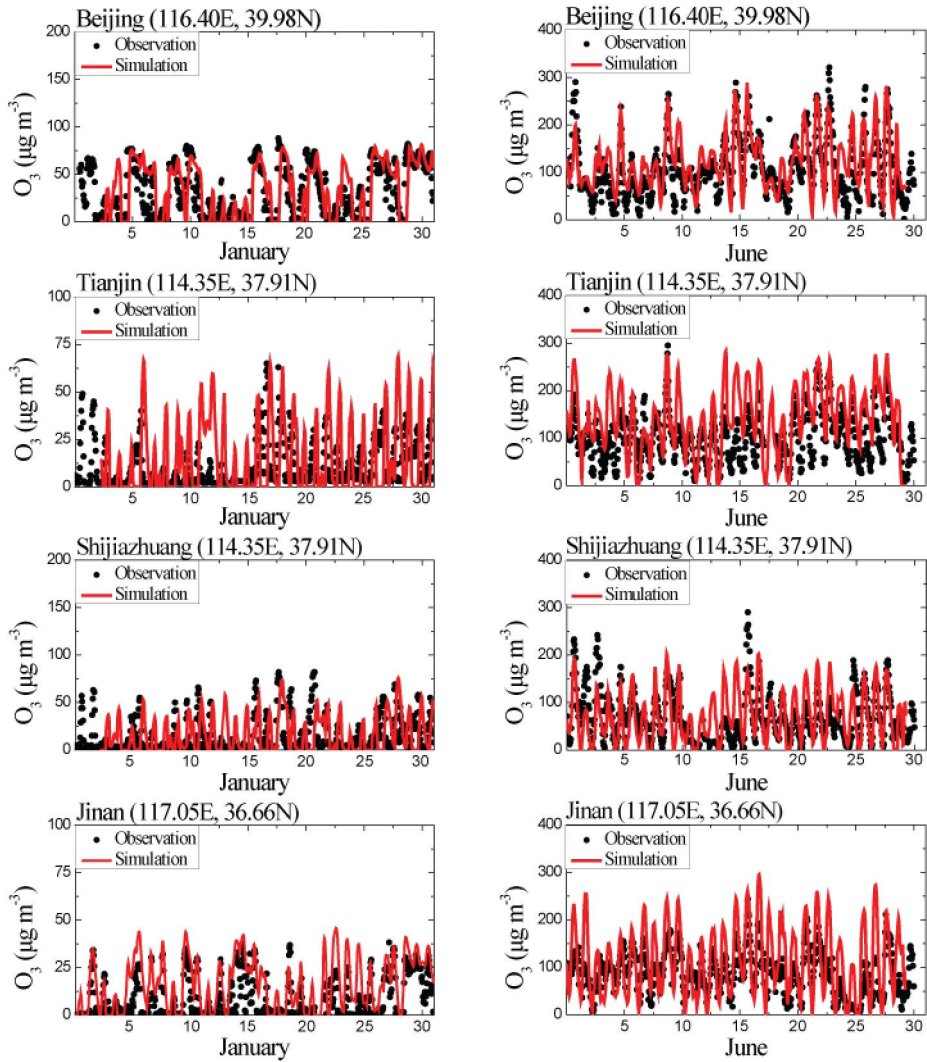
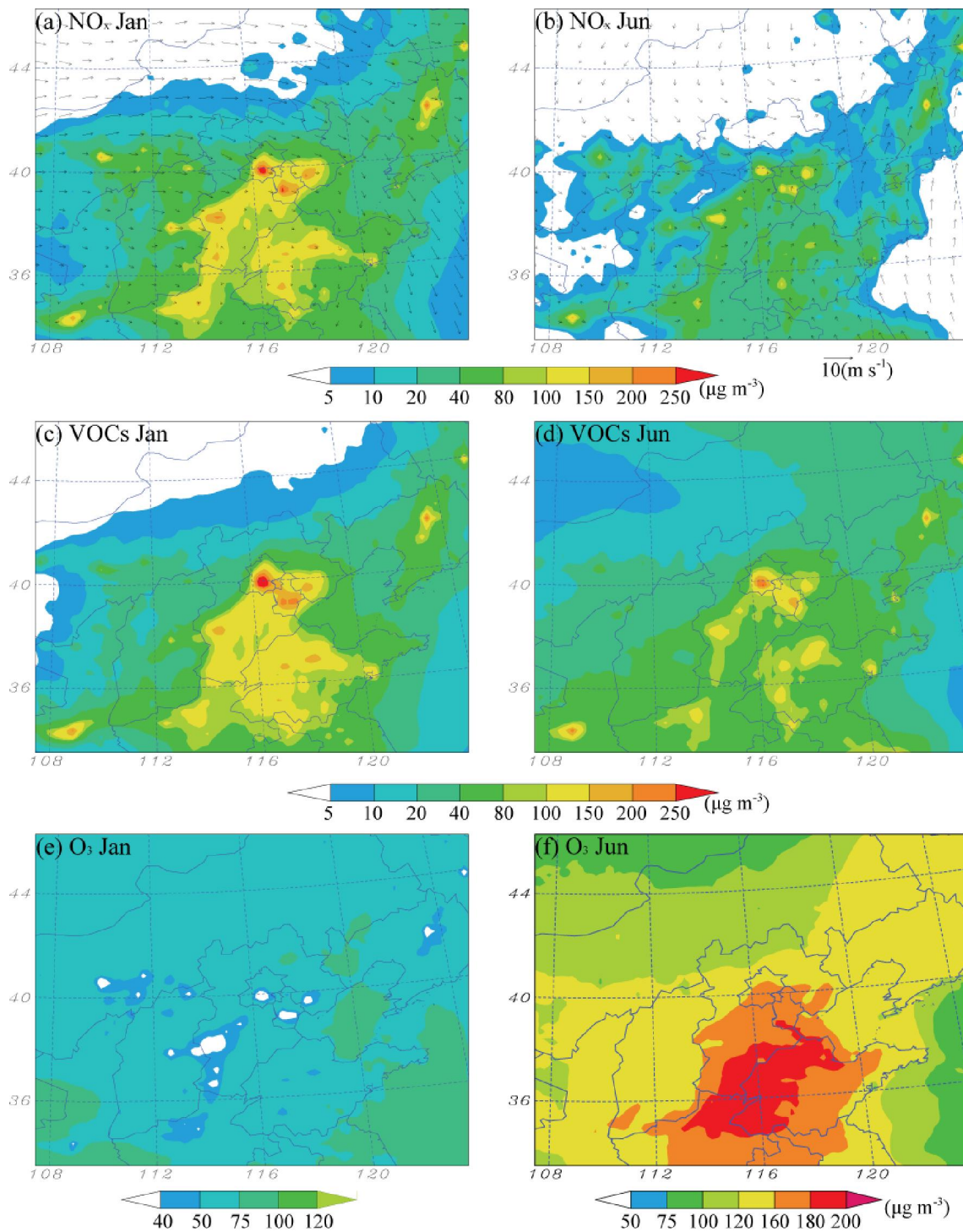


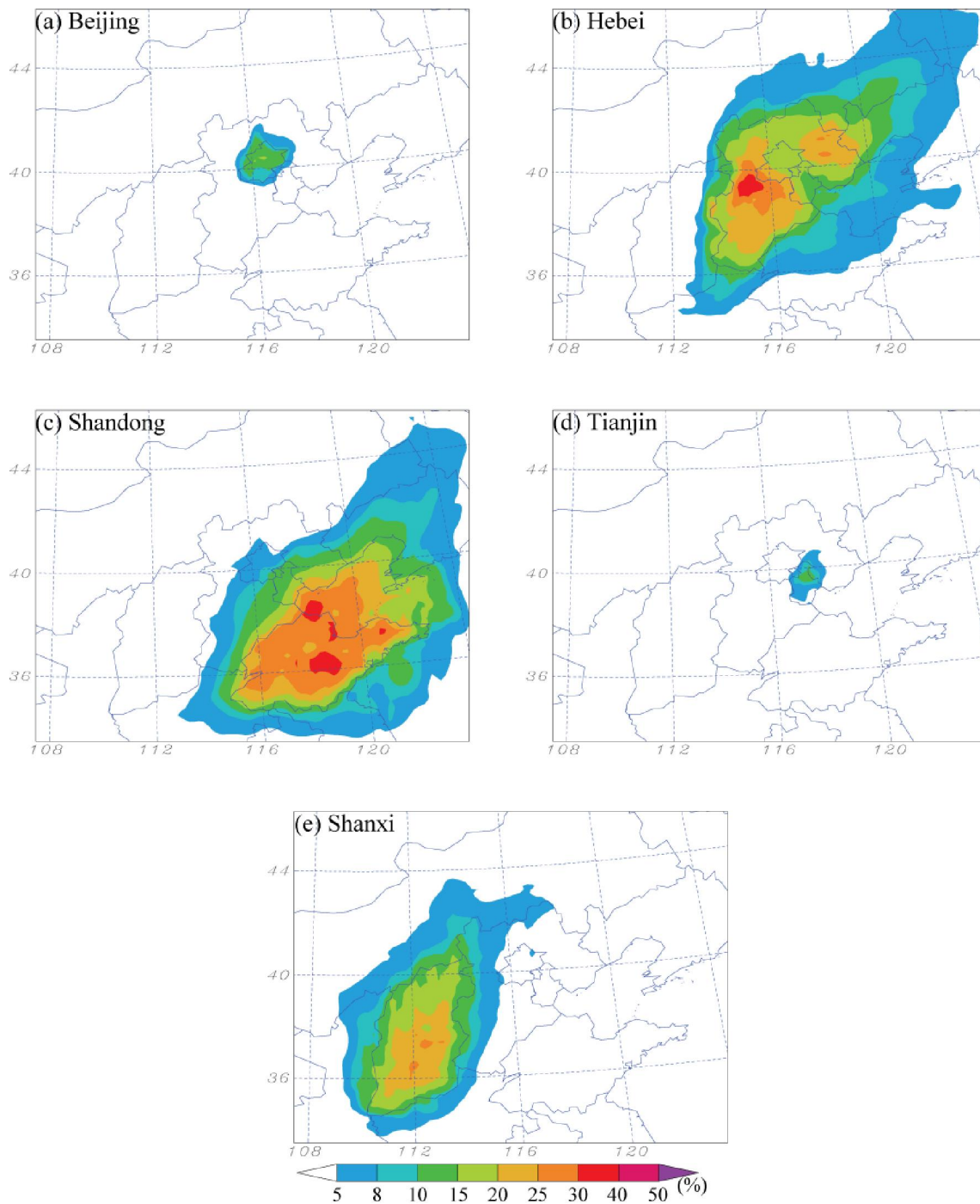
Figure 4. Observed (black circles) and modeled (red solid lines) hourly mass concentrations ($\mu\text{g m}^{-3}$) of O_3 at Beijing, Shijiazhuang, Tianjin, and Jinan in January and June 2015.

652
 653
 654
 655
 656
 657
 658
 659
 660
 661
 662
 663
 664
 665
 666
 667
 668



669
 670 Figure 5. The surface spatial distributions of monthly average NO_x (a-b) and VOCs (c-d), and maximum daily 8H- O_3 (e-
 671 f) in January and June 2015.

672
 673
 674
 675
 676
 677
 678



679 Figure 6. The regional contribution of NO_x-sensitive O₃ from (a) Beijing, (b) Hebei, (c) Shandong, (d) Tianjin, and (e)
 680
 681 Shanxi in June 2015.
 682

679
 680
 681
 682
 683
 684
 685
 686
 687
 688
 689

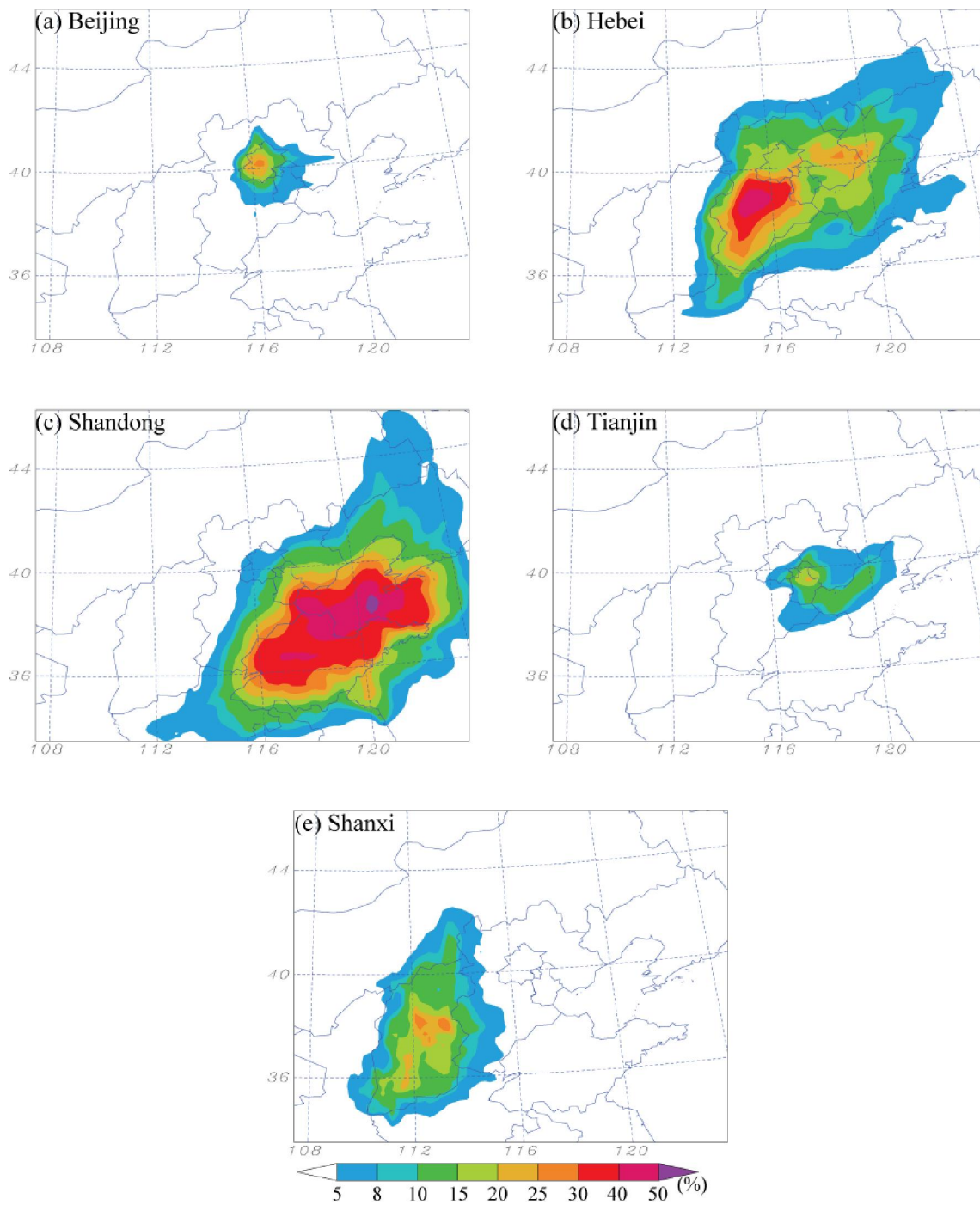


Figure 7. Same as Figure 5 but for VOC-sensitive O_3 .

690
691
692
693
694
695
696
697
698
699
700

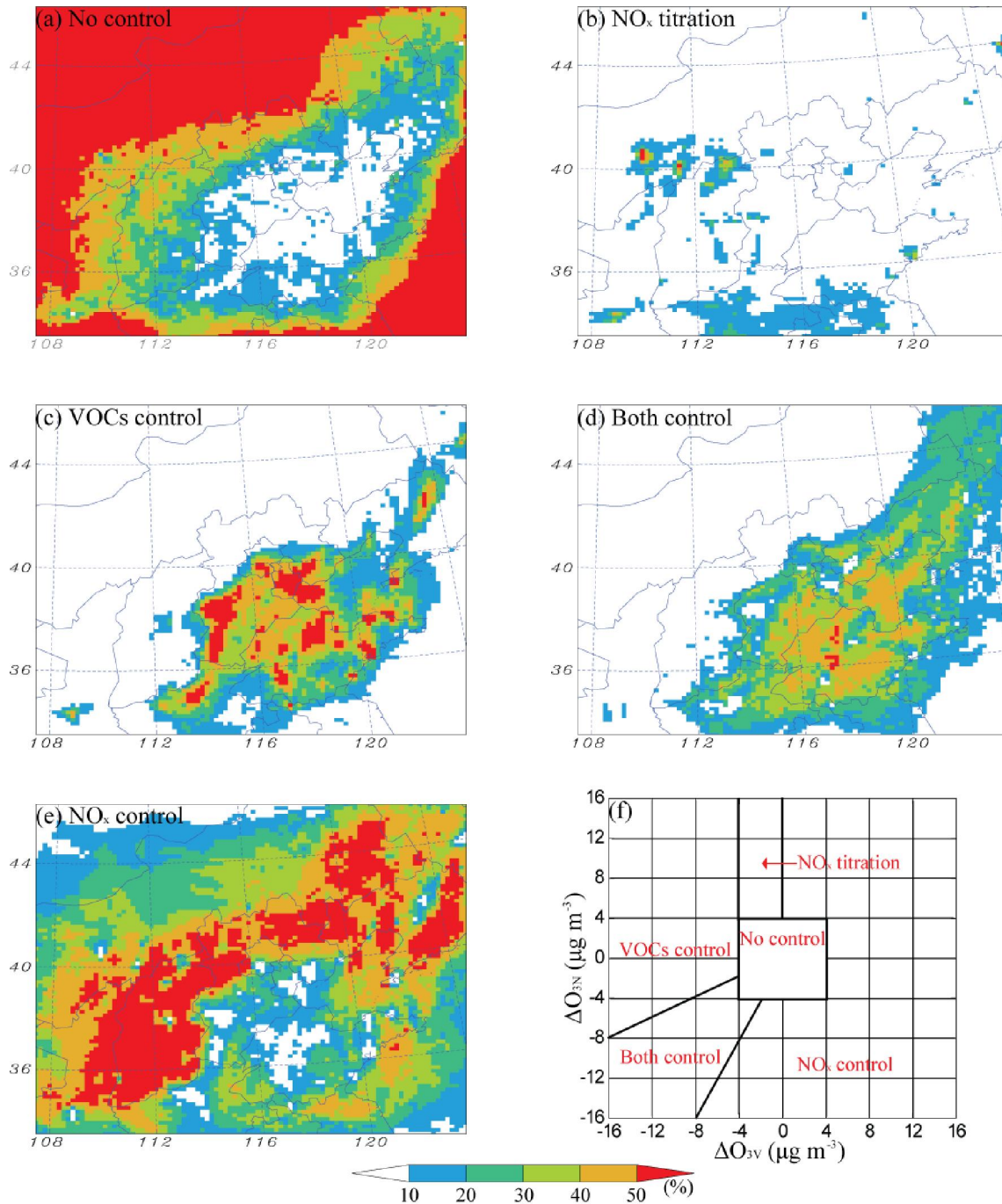


Figure 8. Distributions of the frequency of 8-hour ozone precursor sensitivity regions in June 2015.

701
702
703
704
705
706
707
708
709
710
711
712

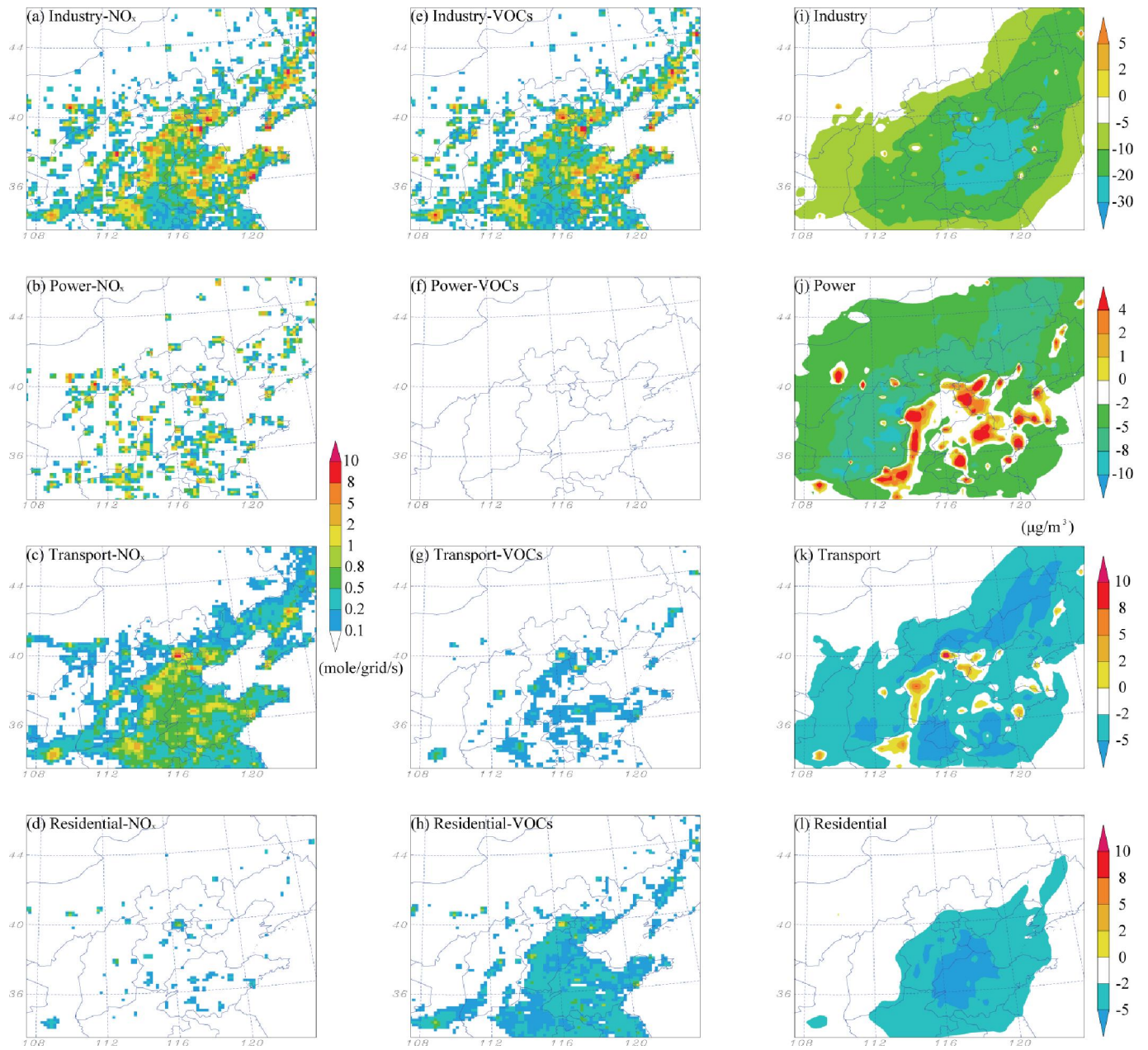
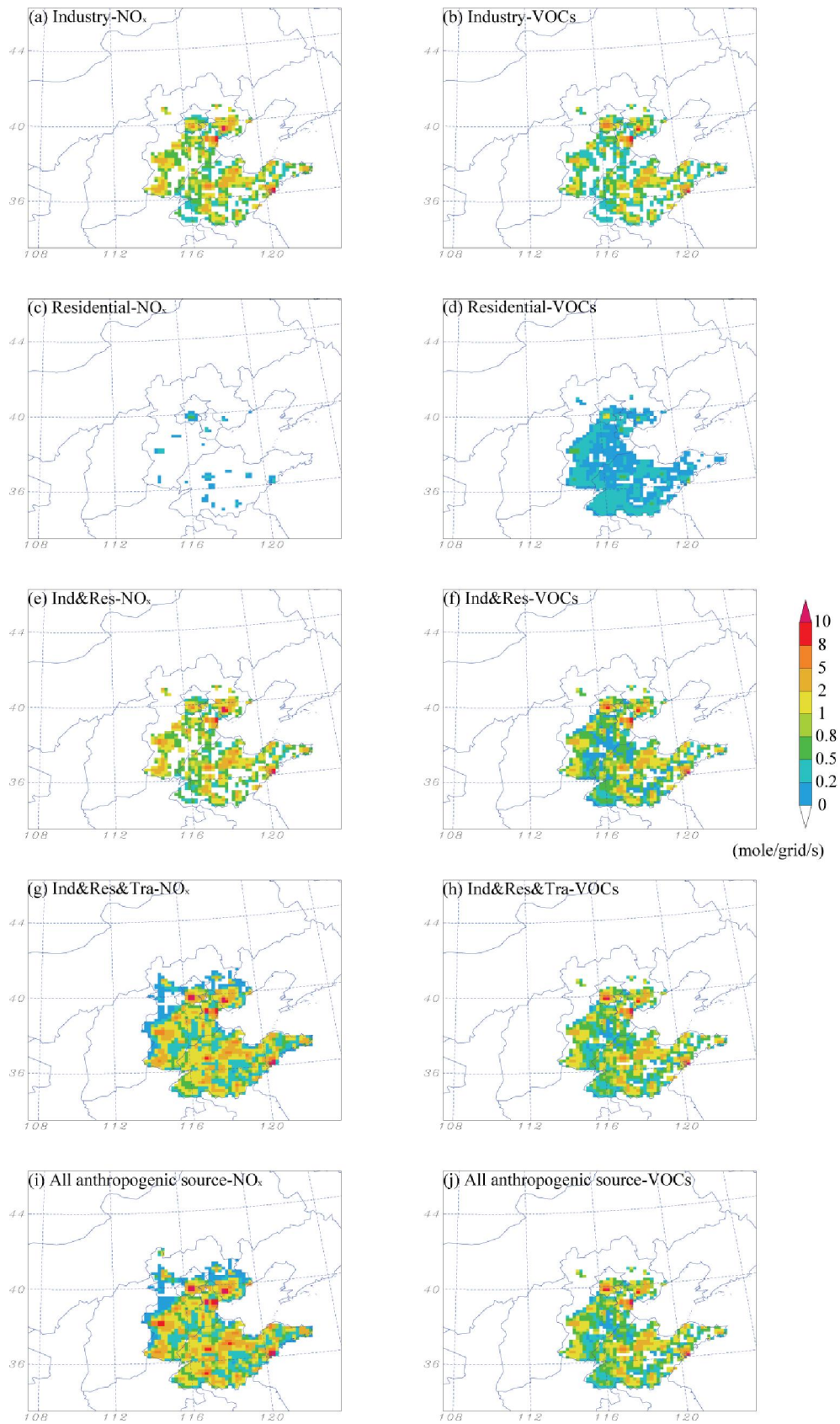


Figure 9. Distributions of the emission flux of NO_x and VOCs and the variation of mass concentration of 8H-O_3 associated with the ZI, ZP, ZT, and ZR in June.

713
714
715
716
717
718
719
720
721
722
723
724
725
726



727

728

729

730

Figure 10. Distributions of the NO_x and VOCs emission flux from different sectors or combinations in the high emission regions of Beijing, Tianjin, Hebei, Shandong in June.

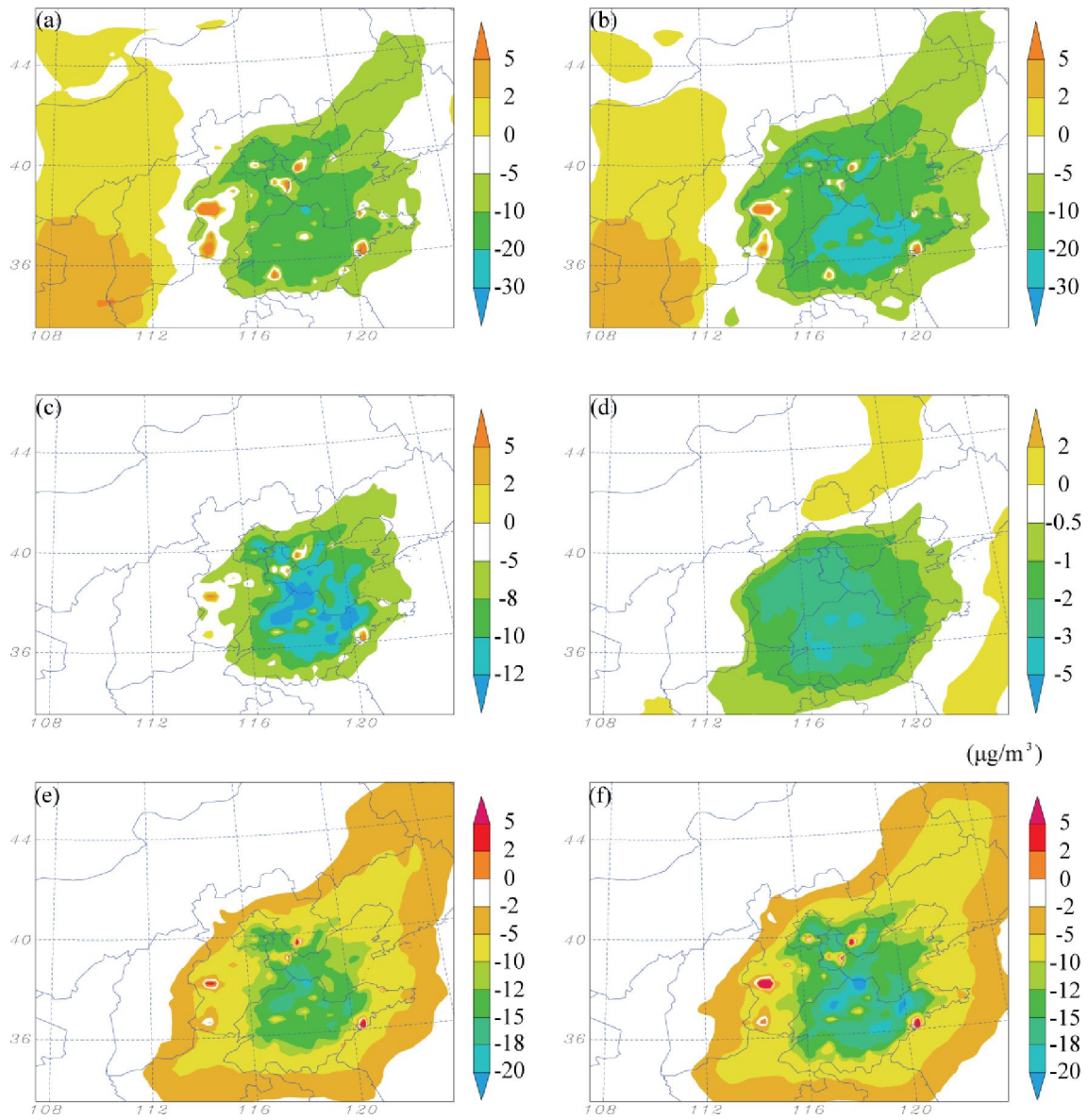


Figure 11. Distributions of the variation of 8H-O₃ mass concentration associated with brute force sensitivity tests: (a) A20%-HER; (b) A20%-BHTS; (c) I20%-HER; (d) R20%-HER; (e) IR20%-HER; (f) ITR20%-HER.

731

732

733

734

735

736

737

738

739

740

741

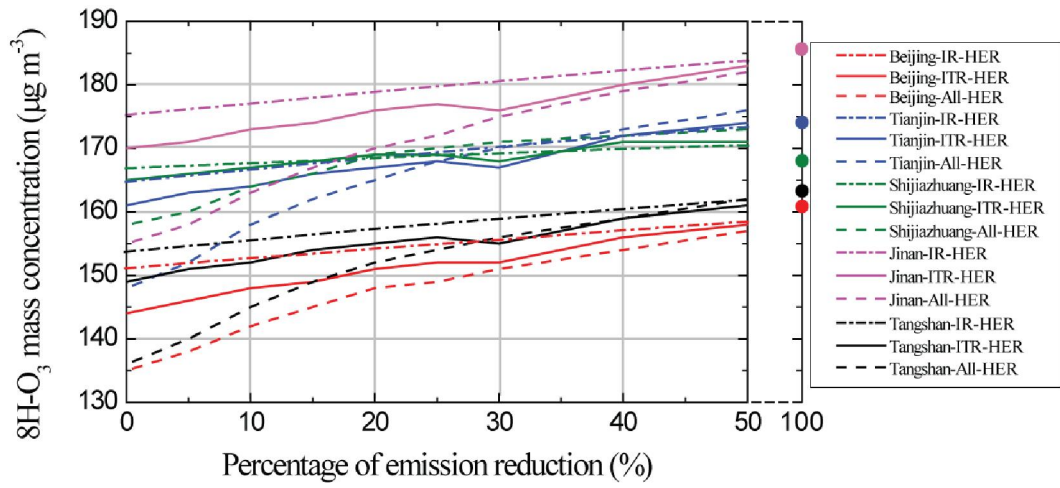
742

743

744

745

746



747
 748 Figure 12. The variation of regional average 8H-O₃ mass concentrations in Beijing, Tianjin, Shijiazhuang, Jinan, and
 749 Tangshan with reduction of IR, ITR and All emissions, respectively.
 750
 751
 752
 753
 754
 755
 756
 757
 758
 759
 760
 761
 762
 763
 764
 765
 766
 767
 768
 769
 770
 771
 772
 773
 774
 775
 776
 777
 778
 779

780

Table 1. Statistical summary of the comparisons of the hourly NO₂ comparison between simulation and observation

		N^a	C_{obs}^b	C_{mod}^c	σ_{obs}^d	σ_{mod}^e	R^f	
NO ₂	Beijing	Jan	602	68.71	50.62	42.98	21.7	0.59
		Jun	588	45.39	46.75	24.95	28.49	0.53
	Jinan	Jan	616	74.39	63.26	33.98	19.55	0.55
		Jun	639	34.27	34.93	19.57	18.76	0.47
	Shijiazhuang	Jan	618	90.04	83.78	44.91	21.55	0.54
		Jun	629	26.11	38.82	21.59	22.26	0.44
	Tianjin	Jan	584	73.73	49.07	37.94	18.52	0.55
		Jun	639	30.02	40.29	18.36	23.25	0.52

781

^a Number of samples

782

^b Total mean of observation

783

^c Total mean of simulation

784

^d Standard deviation of observation

785

^e Standard deviation of simulation

786

^f Correlation coefficient between daily observation and simulation

787

788

789

790

791

792

793

794

795

796

797

798

799

800

801

802

803

804

805

806

807

808

809

810

811

812

813

814

815

Table 2. Statistical summary of the comparisons of the hourly O₃ comparison between simulation and observation

		<i>N</i>	<i>C_{obs}</i>	<i>C_{mod}</i>	<i>σ_{obs}</i>	<i>σ_{mod}</i>	<i>R</i>	
O ₃	Beijing	Jan	615	33.57	37.88	27.58	27.2	0.54
		Jun	676	106.96	120.85	63.75	57.33	0.74
	Jinan	Jan	673	11.09	13.58	10.75	13.08	0.74
		Jun	693	87.91	111.44	45.54	71.8	0.62
	Shijiazhuang	Jan	627	15.24	18.54	18.74	18.7	0.57
		Jun	692	69.53	71.78	53.15	76.14	0.65
	Tianjin	Jan	629	10.83	17.05	11.78	19.36	0.48
		Jun	675	100.42	143.31	52.22	69.48	0.74

816

817

818

819

820

821

822

823

824

825

826

827

828

829

830

831

832

833

834

835

836

837

838

839

840

841

842

843

844

845

846

847

848

849

850
851

852
853
854
855
856
857
858
859
860
861
862
863
864
865
866
867
868
869
870
871
872
873
874
875
876
877
878
879
880
881
882
883
884
885
886
887

Table 3. The regional transport contributions of O₃ mass concentration in Beijing, Tianjin, Hebei, Shandong, Shanxi, and boundary condition (BCON), initial condition (ICON), and other sources (nature sources)

	Beijing	Tianjin	Hebei	Shandong	Shanxi	BCON	ICON	Other
Beijing	23.1%	5.3%	35.2%	13.2%	5.4%	7.3%	0.1%	10.4%
Tianjin	9.0%	14.9%	29.0%	37.3%	3.6%	1.8%	0.1%	4.3%
Hebei	6.3%	5.3%	36.6%	19.4%	7.7%	16.4%	0.1%	8.2%
Shandong	1.3%	2.1%	9.6%	53.6%	3.1%	19.4%	0.1%	10.8%
Shanxi	1.4%	1.4%	10.8%	4.5%	45.0%	22.1%	0.1%	14.7%

Table 4. The brute force sensitivity tests set in this study

	Abbreviation	Brute force sensitivity test
1	ZI	Zero-out of industry emission sector
2	ZP	Zero-out of power plants emission sector
3	ZT	Zero-out of transport emission sector
4	ZR	Zero-out of residential emission sector
5	A20%-BHTS	20% emission of all anthropogenic sectors in BHTS
6	A20%-HER	20% emission of all anthropogenic sectors in the selected high emission regions of BHTS
7	I20%-HER	20% emission of industry sector in the selected high emission regions of BHTS
8	R20%-HER	20% emission of residential sector in the selected high emission regions of BHTS
9	IR20%-HER	20% emission of industry and residential sector in the selected high emission regions of BHTS
10	ITR20%-HER	20% emission of industry, transport, and residential sector in the selected high emission regions of BHTS

889
890
891
892
893
894
895
896
897
898
899
900
901
902
903
904
905
906
907
908
909
910
911
912
913
914
915